International Forum on Aeroelasticity and Structural Dynamics
IFASD 2017
25-28 June 2017, Como-Italy

PARAMETRICALLY RICH NONLINEAR REDUCED-ORDER MODELING: AN APPLICATION IN VISCOUS INCOMPRESSIBLE FLOW

Kim[1], T., Dowell[2], E.H.

[1]Pegase Avtech
Bothell, WA, USA
jxkim3692@gmail.com

[2]Department of Mechanical Engineering and Materials Science
Duke University
Durham, NC, USA
earl.dowell@duke.edu

Keywords: Nonlinear system, modes, dynamic eigenmodes, modally equivalent perturbed system, degenerate transformation, reduced order model

Abstract: In this work, we seek parametrically rich modes that can be used to analyze nonlinear systems for a continuous variation of operating conditions. Towards this end, based on the Modally Equivalent Perturbed System (MEPS) and the Degenerate Transformation (DT) methods, a new and linear perturbed system is formulated and the basis vectors that span a rich nonlinear solution space are obtained from the resulting system of equations. These basis vectors, which obey the principle of linear superposition, lead to a new approach to nonlinear analysis that has the potential for a significant reduction in the complexity of the analysis as well as in computing time. The new scheme is demonstrated using a computational model of a two-dimensional incompressible, viscous flow in which the basis modes are obtained conveniently from snapshots of time responses of the unsteady flow field. It is shown that when used in conjunction with nonlinear reduced-order modeling they produce very accurate results for a wide range of Reynolds numbers and boundary conditions.

1. INTRODUCTION

It is well known that the principle of superposition does not apply to nonlinear systems. One nonlinear solution for one condition is different from another nonlinear solution for another condition, which implies it is difficult to find similarities or scalability between any two nonlinear solutions. This is why solving and analyzing nonlinear equations are so challenging and time consuming. Lately, there has been much effort to circumvent the difficulty by first calculating basis modes for the system and then approximating the solution in a modal expansion with these modes. This approach which is generally known as *modal analysis* comes down to solving a reduced set of equations with respect to the chosen modal coordinates, instead of the original full dimensional equations. Frangos, et. al, [1] gives a good overview of important research milestones in the past. Unfortunately, despite much progress it is still impossible to avoid the fundamental limitation of the nonlinear analysis, that is, the inability to apply the linear superposition. Thus, researchers have seen fit to

execute the so called *Greedy Sampling* by populating the mode set through a rich ensemble of snapshots for multiple conditions which inevitably involves a long computing process [2].

Recently, Kim [3] reported a new finding that may at first seem contradictory and counter-intuitive to the notion about the nature of nonlinear systems. More specifically, it was shown that based on the creation of a Modally Equivalent Perturbed System (MEPS) and a Degenerate Transformation (DT), along with a frequency domain formulation, basis vectors that span a parametrically rich nonlinear solution space can be obtained such that they obey a form of linear superposition. Because they satisfy the linear property, these vectors could lead to a new approach to nonlinear analysis that may result in a significant reduction in the complexity of the analysis as well as in computing time.

In the present work, we introduce another version of this approach which is formulated and solved entirely in the time domain and therefore may be more attractive for some applications. The new scheme is demonstrated using a computational model of a two-dimensional Lid-Driven Cavity Flow in which the basis modes are obtained conveniently from time snapshots of the unsteady flow field. It is shown that when used in conjunction with nonlinear reduced-order modeling they produce very accurate results for a wide range of operating conditions, i.e., Reynolds numbers and lid boundary speeds.

2. STATIC VS. DYNAMIC EIGENMODES

Before embarking on the theoretical development, let us review briefly one of the most commonly performed methods in engineering and science, i.e. modal analysis. In this general approach, to model and find a solution of a physical system described by multiple degrees of freedom we assume that the system response is a linear superposition of certain modes or vectors $\boldsymbol{v}_i$'s and their generalized coordinates, $q_i(t)$'s:

$$\boldsymbol{x}(t) = \boldsymbol{v}_1 q_1(t) + \boldsymbol{v}_2 q_1(t) \ldots + \boldsymbol{v}_R q_R(t) \tag{1}$$

Normally, a small number of modes are included in the expansion so that it can lead to a reduced set of equations approximating the full equations. Among the potential candidates for $\boldsymbol{v}_i$'s are the system eigenmodes for the corresponding linear system. For a well defined system matrix $\boldsymbol{A}$, they satisfy

$$\boldsymbol{A}\boldsymbol{v}_i = \lambda_i \boldsymbol{v}_i \tag{2}$$

Frequently, the physical system is subjected to parameter variations or uncertainties. For example, there may be uncertainty in the modeling. From the design perspective, during an optimization it becomes necessary to permit the design variables to change. On the other hand, if the system is nonlinear different operating points would yield different solutions. The *static* eigenmodes defined as in (2) for one set of model parameters have serious shortcomings in that they cannot account for any changes in the parameters or a nonlinear operating point. One set of the modes are strictly valid only for one set of system properties and a fixed operating condition, although they may be useful for a moderate range of parameter variations IF the system response is not sensitive to a given parameter.

Consider now instead an expansion in which the response is expressed by *dynamic* eigenmodes, $\boldsymbol{v}_i(t)$'s and convolutions between the modes and the generalized coordinates:

$$\boldsymbol{x}(t) = \boldsymbol{v}_1 * a_1 + \boldsymbol{v}_2 * a_2 \ldots + \boldsymbol{v}_R * a_R \tag{3}$$

where * represents the time convolution. The idea is that by allowing the eigenmodes to be *time-varying* and replacing the multiplication $\boldsymbol{v}_i q_i$ with the *convolution* $\boldsymbol{v}_i * q_i$, (3) broadens the range of the modal space, thereby providing an opportunity to capture the continuous parameter variation and nonlinear operating points. Much like the conventional eigenvalue problem, the dynamic eigenmodes may be associated with *dynamic eigenvalues*, $\lambda_i(\omega)$'s:

$$\boldsymbol{T}(\omega)\boldsymbol{v}_i(\omega) = \lambda_i(\omega)\boldsymbol{v}_i(\omega) \tag{4}$$

for a properly defined frequency valued matrix $\boldsymbol{T}(\omega)$. If the idea works *the same set of modes* $\boldsymbol{v}_i(\omega)$'s *will be valid for large variations in the parameters and operating conditions.*

Several questions arise as to the idea of invoking and using the dynamic eigenmodes. First, how should $\boldsymbol{T}(\omega)$ be formulated in a meaningful way such that (3) effectively covers the range of variations in the parameters and operating conditions? Second, how do we determine stability of the system using $\lambda_i(\omega)$'s? Third, are there alternatives to $\boldsymbol{v}_i(t)$'s because calculating the convolutions as given in (3) may be computationally expensive? Lastly, will it be possible to apply to experimental data as well as computational data? Some of these questions have been explored and answered in the recent works [4-5]. In particular, it has been shown and demonstrated that in the case of linear systems a MEPS can be defined and set up so that its dynamic eigenmodes satisfy equation (4). Most recently, this approach has been extended to nonlinear systems as well as time-varying cases leading to the same outcome and benefits that have been proved and demonstrated in the linear cases [3]. Regarding the third question, it is practical and makes sense to approximate the time convolutions in (3) by a plain superposition:

$$\boldsymbol{v}_1 * a_1 + \boldsymbol{v}_2 * a_2 \ldots + \boldsymbol{v}_R * a_R \approx \boldsymbol{\phi}_1 q_1(t) + \boldsymbol{\phi}_2 q_1(t) \ldots + \boldsymbol{\phi}_S q_S(t) \tag{5}$$

For example, modes (not to be confused with the eigenmodes) $\boldsymbol{\phi}_i$'s can be found by processing $\boldsymbol{v}_i(\omega)$'s via the Frequency Domain Karhunen-Loeve Procedure [6] and POD (Proper Orthogonal Decomposition) [7]. Due to the nature of convolution, it is expected that $S > R$, that is, being time-varying the dynamic eigenmodes will spread over a larger range of regular modes.

In the sections to follow, a new procedure for obtaining parametrically rich nonlinear solution space will be introduced following the idea of dynamic eigenmodes. This approach is different from that of [3] in that it is set entirely in the time domain and the nominal system is nonlinear rather than linear, although the important outcomes of the earlier development, i.e., the MEPS and DT, will be utilized in the derivation.

3. THEORETICAL FRAMEWORK

In this section, following the key ideas of the MEPS and DT a brief outline and key highlights of the theoretical development for the proposed modal solutions of nonlinear systems will be presented. For detailed derivations of the MEPS and DT, refer to the supplementary materials attached to Ref. [3].

Given a nonlinear system with multiple degrees of freedom,

$$\dot{\boldsymbol{x}}(t) = \boldsymbol{f}(\boldsymbol{x}) + \boldsymbol{b} \tag{6}$$

where

$$\boldsymbol{f} = (N \times 1)\ nonlinear\ function\ vector$$
$$\boldsymbol{x} \equiv (N \times 1)\ state\ vector$$
$$\boldsymbol{b} \equiv (N \times 1)\ IC\ or\ BC\ or\ Input\ vector$$

we seek for a solution in the form

$$\boldsymbol{x}(t) = \boldsymbol{x}_0(t) + \boldsymbol{\Delta x}(t) \tag{7}$$

where the nominal and perturbed solutions satisfy, respectively,

$$\dot{\boldsymbol{x}}_0 = \boldsymbol{f}(\boldsymbol{x}_0) + \boldsymbol{b}_0 \text{ : Nominal} \tag{8}$$
$$\boldsymbol{\Delta}\dot{\boldsymbol{x}} = \boldsymbol{f}(\boldsymbol{x}) - \boldsymbol{f}(\boldsymbol{x}_0) + \boldsymbol{\Delta b} \text{ : Perturbed} \tag{9}$$

Note that we do not separate – if there is any – the linear part from $\boldsymbol{f}(\boldsymbol{x})$. This is a main departure from the previous work, but will better suit nonlinear systems that do not have well defined linear parts. For instance, the Euler equations of fluid mechanics intrinsically do not have a linear part.

Define $\boldsymbol{\Delta A}(\boldsymbol{x})$ such that

$$\boldsymbol{f}(\boldsymbol{x}) \equiv \boldsymbol{\Delta A}(\boldsymbol{x})\boldsymbol{x} \tag{10}$$

where $\boldsymbol{\Delta A}(\boldsymbol{x})$ satisfies a *Lipschitz condition*:

$$\|\boldsymbol{\Delta A}(\boldsymbol{x}_2) - \boldsymbol{\Delta A}(\boldsymbol{x}_1)\| \leq \alpha(K)\|\boldsymbol{x}_2 - \boldsymbol{x}_1\| \tag{11}$$

It is noted that a selection of $\boldsymbol{\Delta A}(\boldsymbol{x})$ is not unique but can always be found [8]. Then (9) can be rewritten as

$$\boldsymbol{\Delta}\dot{\boldsymbol{x}} = [\boldsymbol{\Delta A}(\boldsymbol{x}_0) + \boldsymbol{\Delta A}_d(\boldsymbol{x}_0, \boldsymbol{\Delta x})]\boldsymbol{\Delta x} + \boldsymbol{\Delta A}_d(\boldsymbol{x}_0, \boldsymbol{\Delta x})\boldsymbol{x}_0 + \boldsymbol{\Delta b} \tag{12}$$

where

$$\boldsymbol{\Delta A}_d(\boldsymbol{x}_0, \boldsymbol{\Delta x}) \equiv \boldsymbol{\Delta A}(\boldsymbol{x}) - \boldsymbol{\Delta A}(\boldsymbol{x}_0) \tag{13}$$

3.1 Modally Equivalent Perturbed System (MEPS)

Following the procedure described in [3], it can be shown that the perturbed system (12) is *modally equivalent* to the following system:

$$\boldsymbol{\Delta \dot{x}'} = \boldsymbol{\Delta A}(\boldsymbol{x}_0)\boldsymbol{\Delta x'} + \boldsymbol{\Delta A}_d(\boldsymbol{x}_0, \boldsymbol{\Delta x'})\boldsymbol{x}_0 + \boldsymbol{\Delta b} \tag{14}$$

As a result, although the two solutions of (12) and (14), $\boldsymbol{\Delta x}$ and $\boldsymbol{\Delta x'}$ are different they share the same set of the *dynamic eigenmodes*, and therefore modes that span the solution space of the perturbed system can be found by solving the MEPS (14) instead of solving the original (12). See Figure 1 for a graphical description of the MEPS.

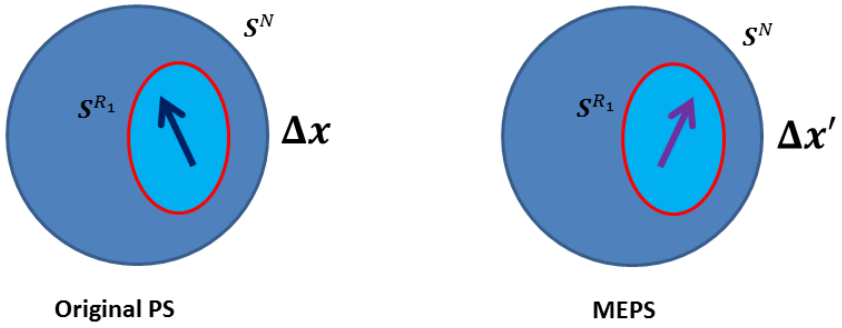

Figure 1 Solution space shared by the original (left) and MEPS (right) solutions, Δx and $\Delta x'$.

Originally, the MEPS was derived for time-invariant linear systems undergoing parameter variations based on the Dynamic Eigen Decomposition and Cayley-Hamilton Theorem, and was used in constructing Parametric Reduced-Order Model (PROM) [4-5]. More recently, the analysis was extended to time-varying cases treating $\boldsymbol{\Delta A}(\boldsymbol{x})$ as time-varying parameters and using frequency-domain convolution [3]. In the above, we treat both $\boldsymbol{\Delta A}(\boldsymbol{x}_0)$ and $\boldsymbol{\Delta A}_d(\boldsymbol{x}_0, \boldsymbol{\Delta x'})$ as such**,**

$$\begin{aligned} \boldsymbol{\Delta A}(\boldsymbol{x}_0) &\equiv \boldsymbol{\Delta A}(t) \\ \boldsymbol{\Delta A}_d(\boldsymbol{x}_0, \boldsymbol{\Delta x'}) &\equiv \boldsymbol{\Delta A}_d(t) \end{aligned} \tag{15}$$

It is noteworthy that the mechanism that derives the nonlinear system and ultimately leads to the MEPS is the *Dynamic Eigen Decomposition* (which was introduced earlier in Eq. (4)). In this light, let us examine closely the eigen structure of the frequency solution of the perturbed equation. Taking Fourier Transform of the time-varying Eq. (12) gives

$$j\omega\,\boldsymbol{\Delta X}(\omega) = \int_{-\infty}^{\infty} [\boldsymbol{\Delta \mathcal{A}}(\omega-\omega') + \boldsymbol{\Delta \mathcal{A}}_d(\omega-\omega')]\boldsymbol{\Delta X}(\omega')d\omega' + \int_{-\infty}^{\infty} \boldsymbol{\Delta \mathcal{A}}_d(\omega-\omega')\boldsymbol{X}_0(\omega')d\omega' + \boldsymbol{\Delta b} \quad (16)$$

Given $M+1$ uniformly distributed frequencies $0,\ \omega_1,\ \omega_2,\ \ldots, \omega_M\ \ (\omega_i \equiv i\Delta\omega,\ \omega_M = \Omega_f)$ (16) can be written in compact form,

$$(\bar{\boldsymbol{I}}_{\bar{\boldsymbol{\omega}}} - \overline{\boldsymbol{\Delta \mathcal{A}}} - \overline{\boldsymbol{\Delta \mathcal{A}}}_d)\overline{\boldsymbol{\Delta X}} = \overline{\boldsymbol{\Delta \mathcal{A}}}_d(\bar{\boldsymbol{X}}_0 + \overline{\boldsymbol{\Delta \mathcal{A}}}_{\boldsymbol{d}}^{-p}\overline{\boldsymbol{\Delta b}}) \quad (17)$$

where $\bar{\boldsymbol{I}}_{\bar{\boldsymbol{\omega}}}, \overline{\boldsymbol{\Delta \mathcal{A}}}$, $\overline{\boldsymbol{\Delta \mathcal{A}}}_d$ are $(2M+1)N \times (2M+1)N$ frequency-valued matrices of the augmented dimension. Its solution is obtained as

$$\overline{\boldsymbol{\Delta X}} = (\bar{\boldsymbol{I}}_{\bar{\boldsymbol{\omega}}} - \overline{\boldsymbol{\Delta \mathcal{A}}} - \overline{\boldsymbol{\Delta \mathcal{A}}}_d)^{-1}\overline{\boldsymbol{\Delta \mathcal{A}}}_d(\bar{\boldsymbol{X}}_0 + \overline{\boldsymbol{\Delta \mathcal{A}}}_{\boldsymbol{d}}^{-p}\overline{\boldsymbol{\Delta b}}) \quad (18)$$

Taking eigen decomposition of the transfer function,

$$[\bar{\boldsymbol{I}}_{\bar{\boldsymbol{\omega}}} - \overline{\boldsymbol{\Delta \mathcal{A}}}(\bar{\boldsymbol{\omega}}) - \overline{\boldsymbol{\Delta \mathcal{A}}}_d(\bar{\boldsymbol{\omega}})]^{-1}\overline{\boldsymbol{\Delta \mathcal{A}}}_d(\bar{\boldsymbol{\omega}}) \equiv \bar{\boldsymbol{V}}_\nu(\bar{\boldsymbol{\omega}})\bar{\boldsymbol{\Lambda}}_\nu(\bar{\boldsymbol{\omega}})\overline{\boldsymbol{W}}_\nu^T(\bar{\boldsymbol{\omega}}) \quad (19)$$

where

$$\begin{aligned} \bar{\boldsymbol{\Lambda}}_\nu &= (\nu \times \nu) \text{ diagonal matrix with nonzero eigenvalues} \\ \bar{\boldsymbol{V}}_\nu, \overline{\boldsymbol{W}}_\nu &= \text{right and left eigenvectors} \end{aligned} \quad (20)$$

all of which are not constants but vary with frequency (and time). Hence, they are called the *dynamic eigenmodes*. Using the Cayley-Hamilton's theorem [9] it can be shown that (19) has the same dynamic eigenmodes as the following transfer function:

$$[\bar{\boldsymbol{I}}_{\bar{\boldsymbol{\omega}}} - \overline{\boldsymbol{\Delta \mathcal{A}}}(\bar{\boldsymbol{\omega}})]^{-1}\overline{\boldsymbol{\Delta \mathcal{A}}}_d(\bar{\boldsymbol{\omega}}) \equiv \bar{\boldsymbol{V}}_\nu(\bar{\boldsymbol{\omega}})\bar{\boldsymbol{\Lambda}}'_\nu(\bar{\boldsymbol{\omega}})\overline{\boldsymbol{W}}_\nu^T(\bar{\boldsymbol{\omega}}) \quad (21)$$

except that the two sets of the dynamic eigenvalues are related via

$$\bar{\boldsymbol{\Lambda}}'_\nu \equiv (\bar{\boldsymbol{I}}_\nu + \bar{\boldsymbol{\Lambda}}_\nu)^{-1}\bar{\boldsymbol{\Lambda}}_\nu \quad (22)$$

We recognize that the system which has (21) as the extended Fourier Transform is indeed the perturbed system expressed in (14). Therefore, we conclude that (12) and (14) are modally equivalent.

3.2 Degeneration Transformation (DT)

Another feature of the nonlinear modal analysis introduced is the DT [3]. It was shown through a series of polynomial expansions and MEPS transformations that the perturbed variable $\boldsymbol{\Delta x'}$ appearing in the forcing term of the MEPS equation (14) can be ignored without affecting the modal property of its solution. This is because its effect is canceled by its presence in the homogeneous part of the equation. Note,

$$\begin{aligned}\boldsymbol{\Delta \dot{x}'} &= \boldsymbol{\Delta A}(\boldsymbol{x}_0)\boldsymbol{\Delta x'} + \boldsymbol{\Delta A_d}(\boldsymbol{x}_0, \boldsymbol{\Delta x'})\boldsymbol{x}_0 + \boldsymbol{\Delta b} \\ &= \boldsymbol{\Delta A}(\boldsymbol{x}_0)\boldsymbol{\Delta x'} + \boldsymbol{\Delta A}(\boldsymbol{x}_0 + \boldsymbol{\Delta x'})\boldsymbol{x}_0 - \boldsymbol{f}(\boldsymbol{x}_0) + \boldsymbol{\Delta b}\end{aligned} \tag{23}$$

Applying the DT, $\boldsymbol{\Delta x'}$ in the second term is dropped, the two inner terms cancel each other, and we reach the following new system:

$$\boldsymbol{\Delta \dot{x}}'' = \boldsymbol{\Delta A}(\boldsymbol{x}_0)\boldsymbol{\Delta x}'' + \boldsymbol{\Delta b} \tag{24}$$

However, in solving (24) we desire $\boldsymbol{\Delta x}''$ to be *dimensionally rich.* This is possible if we let the matrix differential at a nominal point $\boldsymbol{\Delta A}(\boldsymbol{x}_0)$ be *rich*. Thus, $\boldsymbol{x}_0$ is replaced with $\boldsymbol{\Phi}_0\boldsymbol{r}_0$ where

$$\begin{aligned}\boldsymbol{r}_0(t) &\equiv \boldsymbol{\Phi}_0^T\bar{\boldsymbol{x}}_0 + \boldsymbol{w}(t) \\ \bar{\boldsymbol{x}}_0 &\equiv mean(\boldsymbol{x}_0(t)) \\ \boldsymbol{w}(t) &\equiv uncorrelated\ randon\ signals\end{aligned} \tag{25}$$

with $\|\boldsymbol{w}\|_{std} = \|\boldsymbol{\Phi}_0^T(\boldsymbol{x}_0 - \bar{\boldsymbol{x}}_0)\|_{std}$, $mean\big(\boldsymbol{w}(t)\big) = 0$. The vector space spawned by nonlinear solutions of (6) now comprises those of the nominal system equation (8) and yet another perturbed equation (24).

4. LINEARITY AND SUPERPOSITION

It is immediately noted that although it started out as a nonlinear equation there is nothing nonlinear about the perturbed equation (24) because once $\boldsymbol{x}_0$ is known the equation becomes linear though time-varying, an outcome of the MEPS transformation followed by the DT. Consequently, one can expect that the principle of superposition will be satisfied and its solution will yield a parametrically rich vector space containing a continuous set of the nonlinear solutions that cover not only the nominal operating point in (8) but all others away from. The nominal equation (8) is still nonlinear, but since the accompanying (24) is linear, there will be no strict limit as to how much the two equations together can steer away from the nominal operating point and extrapolate beyond. What is revealing is that in the course of seeking for the nonlinear solution space, the nonlinearity of the original equation has been lifted. Importantly, Eq. (24) will generate the same (invariant) dynamic eigenmodes for all scalar multiples of $\boldsymbol{\Delta b}$**.** Hence, by setting $\boldsymbol{b}_0 = \boldsymbol{\Delta b} = \boldsymbol{b}$, it is possible to produce a single vector space containing all the solutions for inputs $\alpha_i\boldsymbol{b}$ $(\alpha_i > 1, i = 1,2, \dots)$. Similarly, one can seek out a vector space due to multiple different inputs or boundary conditions, $\boldsymbol{b}_i$ $(i = 1,2, \dots K)$ by having the system subject to a simultaneous excitation of all the inputs,

$$\boldsymbol{\Delta\dot{x}}'' = \boldsymbol{\Delta A}(\boldsymbol{x}_0)\boldsymbol{\Delta x}'' + \sum_{i=1}^{K} \boldsymbol{\Delta b}_i \, r_i(t) \tag{26}$$

with $\boldsymbol{\Delta b}_i \equiv \boldsymbol{b}_i - \boldsymbol{b}_0$ and $r_i(t)$'s are statistically uncorrelated time signals. The resulting modes will span a rich vector space of all the individual solutions due to $\boldsymbol{b}_i$'s. It is also noteworthy that despite the notion of dynamic eigenmodes used in the derivation, the time convolution in the modal expansion (3) was not necessary and was indeed replaced by the regular expansion as invoked by (5).

5. CALCULATION OF MODES FOR NONLINEAR SYSTEM

As a summary, we describe a procedure to calculate a set of modes that span a parametrically rich vector space for the nonlinear system given in Eq. (6). As opposed to the procedure given in Ref. [3], all the calculations are done in time domain, but as in the frequency-domain formulation the underlying linearity shapes the problem solution.

1. Set a nominal input (or BC) $\boldsymbol{b}_0$ and solve the nominal system Eq. (8).
2. Using the time history data of $\boldsymbol{x}_0$, calculate POD modes set $\boldsymbol{\Phi}_0 = [\, \boldsymbol{\phi}_0^1 \;\; \boldsymbol{\phi}_0^2 \; ... \; \boldsymbol{\phi}_0^{R_0} \,]$.
3. Define $\boldsymbol{\Delta A}(\boldsymbol{x})$ such that $\boldsymbol{f}(\boldsymbol{x}) = \boldsymbol{\Delta A}(\boldsymbol{x})\boldsymbol{x}$.
4. Substitute $\boldsymbol{x}_0$ with $\boldsymbol{\Phi}_0\boldsymbol{r}_0(t)$ where $\boldsymbol{r}_0(t)$ is $(R_0 \times 1)$ random signals vector according to (25), and solve
$$\boldsymbol{\Delta\dot{x}}'' = \boldsymbol{\Delta A}(\boldsymbol{\Phi}_0\boldsymbol{r}_0)\boldsymbol{\Delta x}'' + \boldsymbol{\Delta b} \text{ or } \boldsymbol{\Delta\dot{x}}'' = \boldsymbol{\Delta A}(\boldsymbol{\Phi}_0\boldsymbol{r}_0)\boldsymbol{\Delta x}'' + \sum_{i=1}^{K} \boldsymbol{\Delta b}_i \, r_i.$$
5. Using the time history data of $\boldsymbol{\Delta x}''$**,** calculate POD modes set $\boldsymbol{\Phi}_1 = [\, \boldsymbol{\phi}_1^1 \;\; \boldsymbol{\phi}_1^2 \; ... \; \boldsymbol{\phi}_1^{R_1} \,]$.
6. Get the global modest set, $\boldsymbol{\Phi} = [\boldsymbol{\Phi}_0 \;\; \boldsymbol{\Phi}_1]$. Gram-Schmidt orthogonalization may be necessary to ensure linear independence and orthogonality of the obtained modes.

6. NONLINEAR REDUCED-ORDER MODEL

It is natural to consider a reduced-order model of the original full-order model once basis vectors $\boldsymbol{\phi}_i$'s are obtained. As usual, a ROM can be constructed by $\boldsymbol{x} = \sum_{i=1}^{R} \boldsymbol{\phi}_i q_i$ and projecting the residual vector onto $\boldsymbol{S}^R$ via Galerkin:

$$\dot{\boldsymbol{q}}(t) = \boldsymbol{f}_R(\boldsymbol{\Phi q}) + \boldsymbol{b}_R \tag{27}$$

where

$$\begin{aligned} \boldsymbol{f}_R &\equiv \boldsymbol{\Phi}^T \boldsymbol{f} \\ \boldsymbol{b}_R &\equiv \boldsymbol{\Phi}^T \boldsymbol{b} \end{aligned} \tag{28}$$

As can be expected, much computing will be consumed in executing the key vector product, $\boldsymbol{\Phi}^T \boldsymbol{f}_R(\boldsymbol{\Phi q})$ at every time step. As matter of fact, due to this limitation the nonlinear ROM might even take longer than FOM unless the vector multiplication is done efficiently. The ROM construction is not the main focus of the present work and interested readers may find ample research on nonlinear ROM in the literature [1]. Of particular interest is a Petrov-Galerkin projection that allows accurate estimation of the vector projection, and DEIM

(Discrete Empirical Interpolation Method) [10-11] that minimizes the CPU time and memory during the calculation of $\boldsymbol{\Phi}^T \boldsymbol{f}_R(\boldsymbol{\Phi})$. According to the latter, the vector product is approximated via a least-square scheme:

$$\boldsymbol{\Phi}^T \boldsymbol{f}(\boldsymbol{\Phi q}) \cong \boldsymbol{\Phi}_P^T \boldsymbol{f}_P(\boldsymbol{\Phi q}) \tag{29}$$

where only *P* rows of the matrices are extracted:

$$\boldsymbol{\Phi}_P^T \equiv \boldsymbol{\Phi}^T \boldsymbol{\Psi} \boldsymbol{\Psi}_P^{-1} \;\; (P \ll N) \tag{30}$$

And where $\boldsymbol{\Psi}$ are the basis vectors of $\boldsymbol{f}(\boldsymbol{x})$. In the present work, since our aim is to demonstrate the calculation of the modes, we did not employ an efficient scheme such as DEIM but directly executed the vector multiplication in the time integration.

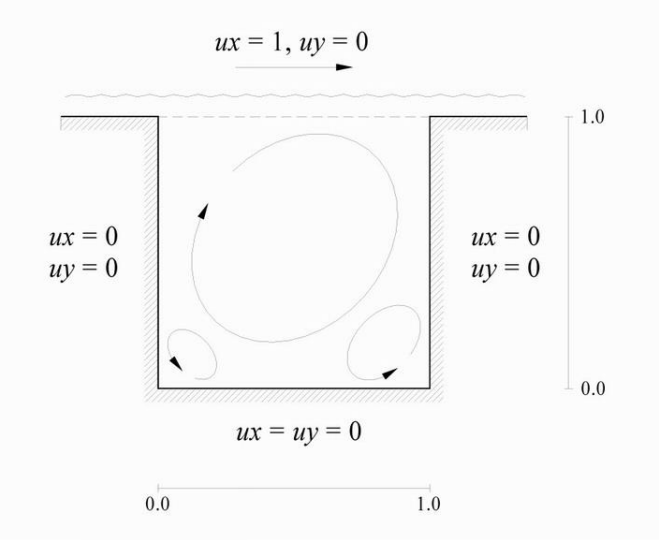

Figure 2 2D incompressible, viscous flow in a reservoir.

7. NEMERICAL EXAMPLE: 2D Lid-Driven Cavity Flow

For demonstration of the parametrically rich modal solution method presented in the previous sections, we apply the technique to a two-dimensional incompressible, viscous flow in a reservoir, namely the 2D Lid-Driven Cavity Flow. The lid driven cavity is a frequently used example for demonstrating new theory and algorithms. In References [12] and [13], this example is studied using a standard POD method as well as a new POD method. Other fluid flow examples are also considered in these references. The goal of the work in [12-13] is to reduce the number of degrees of freedom to as small a number as possible without any essential loss in accuracy for a single set of parameters. Thus that work is complementary to that of the present paper which seeks a reduced order model that may be used for a broad range of system parameters, but may not be the minimal order for any single set of parameters. The present application is limited to laminar viscous flows at relatively low Reynolds numbers although the lid driven cavity has been studied at higher Reynolds numbers where the laminar flow becomes unstable which leads to a limit cycle oscillation and then to chaotic or turbulent flow at even higher Reynolds numbers. Figure 2 shows the geometry of the cavity

and the flow inside it. One wall of the cavity (the lid) moves with a specified velocity which excites oscillations in the cavity.

7.1 Nonlinear Differential Equations for Cavity Flow

Governing fluid dynamic equations are

$$\begin{aligned} \boldsymbol{\nabla \cdot v} &= \mathbf{0} && : \quad \text{Continuity} \\ \frac{\partial \boldsymbol{v}}{\partial t} + \boldsymbol{v \cdot \nabla v} &= -\frac{1}{\rho}\boldsymbol{\nabla p} + \nu \boldsymbol{\nabla^2 v} && : \quad \text{Momentum} \end{aligned} \tag{31}$$

which defining the vorticity and the stream function as

$$\begin{aligned} \boldsymbol{\omega} &= \boldsymbol{\nabla \times v} && : \quad \text{vorticity} \\ \boldsymbol{u} = \frac{\partial \boldsymbol{\psi}}{\partial \boldsymbol{y}}, \quad \boldsymbol{v} &= -\frac{\partial \boldsymbol{\psi}}{\partial \boldsymbol{x}} && : \quad \text{stream function} \\ \boldsymbol{\omega} &= \boldsymbol{\nabla^2 \psi} \end{aligned} \tag{32}$$

yield,

$$\frac{\partial \boldsymbol{\omega}}{\partial t} + \boldsymbol{u}\frac{\partial \boldsymbol{\omega}}{\partial \boldsymbol{x}} + \boldsymbol{v}\frac{\partial \boldsymbol{\omega}}{\partial \boldsymbol{y}} = \nu \boldsymbol{\nabla^2 \omega} \tag{33}$$

Or in terms of solely the stream function,

$$\frac{\partial}{\partial t}\nabla^2\psi + \frac{\partial \psi}{\partial y}\frac{\partial}{\partial x}\nabla^2\psi - \frac{\partial \psi}{\partial x}\frac{\partial}{\partial y}\nabla^2\psi = \nu\nabla^4\psi \tag{34}$$

The right-hand side of (33) represents the linear viscous term, while the second and third terms on the left-hand side are the nonlinear convective terms.

7.2 Discretization and Nonlinear State-Space Equation

To generate state-space equations, Eq. (33) along with the last of (32) is discretized in the $x - y$ plane using equally distributed elements in each direction. This results in the following matrix equation:

$$\boldsymbol{x}^{n+1} = \nu \boldsymbol{A x}^n + \boldsymbol{f}(\boldsymbol{x}^n) + U_{top}\boldsymbol{b} \tag{35}$$

where

$$\boldsymbol{A} \equiv diffusive$$
$$\boldsymbol{f}(\boldsymbol{x}) \equiv convective$$
$$\boldsymbol{b} \equiv lid\ boundary\ condition$$
$$U_{top} \equiv top\ boundary\ velocity$$
$$\nu \equiv viscosity$$

It can be seen that in (33) the convective nonlinear terms are quadratic in $\boldsymbol{x}$. Hence, a linear $\boldsymbol{\Delta A}(\boldsymbol{x})$ can be defined such that it contains the constant matrix $\nu\boldsymbol{A}$. Since Reynolds number is given as $Re \equiv \frac{L_y U_{top}}{\nu}$, changing the number will affect both the linear and the boundary condition terms. In the current study, for simplicity we fix $\frac{L_y}{\nu} = 200$ while varying the lid top boundary speed, U_{top}. Hence, $Re = 200U_{top}$ and only the lid velocity boundary condition will change proportionally the Reynolds number. Total of 60 equal elements are placed along the *x* and *y* axes resulting in 3,540 unknown states in $\boldsymbol{x}$.

7.3 Calculation of Nonlinear Vector Space and Reduced-Order Model

First, a nominal operating point is defined to be at Re =200 and $U_{top} = 1$. For the nominal flow condition chosen, the system Eq. (8) is solved by integrating the equation at 1,000 equally distributed time steps with $\Delta t = .005\ sec$. The resulting time history data is then processed using POD and this yields 48 modes for the set $\boldsymbol{\Phi}_0$ when all of the linearly independent modes are taken (which is usually indicated by the rank of the covariant matrix). Next, the second modes set $\boldsymbol{\Phi}_1$ is calculated using the procedure described in Section 5. and Eq. (24). Note that we set $\boldsymbol{\Delta b} = \boldsymbol{b}$ because the boundary term is only changing by the scalar, U_{top}. After examining eigenvalue distribution of the POD covariance matrix carefully, 458 modes are selected for $\boldsymbol{\Phi}_1$. This number, if less than the rank of the covariance matrix, is somewhat arbitrary but always can be chosen to be big enough to give accurate results. After orthogonalizing using the Gram-Schmidt, 505 modes are obtained for the total modes set $\boldsymbol{\Phi} = [\boldsymbol{\Phi}_0\ \boldsymbol{\Phi}_1]$. Thus, $\boldsymbol{\Phi}$ is (3540×505).

The nonlinear ROM discussed in Section 6. is constructed by a Galerkin method. As mentioned earlier, no attempt has been made to minimize the computing time required in carrying out the vector multiplication $\boldsymbol{\Phi}^T\boldsymbol{f}$ in Eq. (27). However, it was reported previously that executing DEIM does reduce the computation although the saving is only marginal for the flow conditions under consideration. In order for the nonlinear ROMs to be effective further research is necessary to implement the scheme for the present formulation and estimate how much computational time can be saved using the scheme.

7.4 Numerical Results: FOM vs. ROM

Figure 3 is a velocity profile within the cavity for the simulated nominal flow condition $Re = 200$ at $t = 5\ sec$ after the uniform speed $U_{top} = 1$ has been applied at the top. It was obtained using the original full model. Figure 4 is the velocity file obtained by solving the ROM that was constructed using the 505 modes. Figures 5 and 6 are the corresponding horizontal (U) and vertical (V) velocity components along the vertical line at the center of the

cavity. Also presented here are results from another ROM that was built using just the nominal 48 modes. As expected, an excellent agreement between all three models is seen in the figures. The real question is, how well will these ROMs capture the flow field when the key parameter, i.e. the Reynolds number changes? To answer this question, U_{top} is increased and the results of the ROMs are examined again.

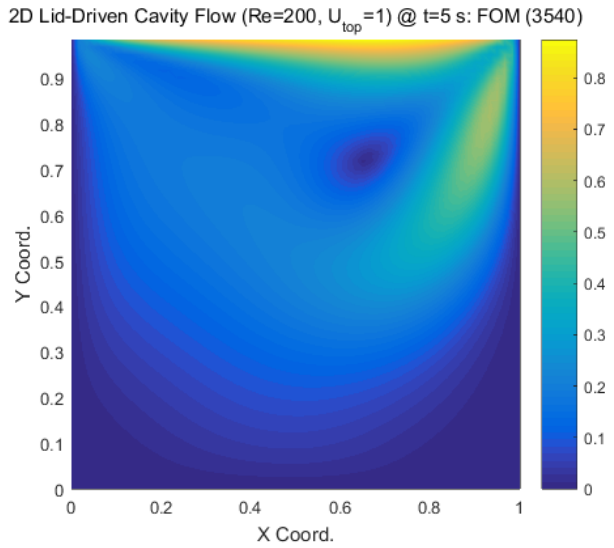

Figure 3 Velocity profile by FOM: $Re = 200$, $U_{top} = 1$ (nominal) at $t = 5\ sec$.

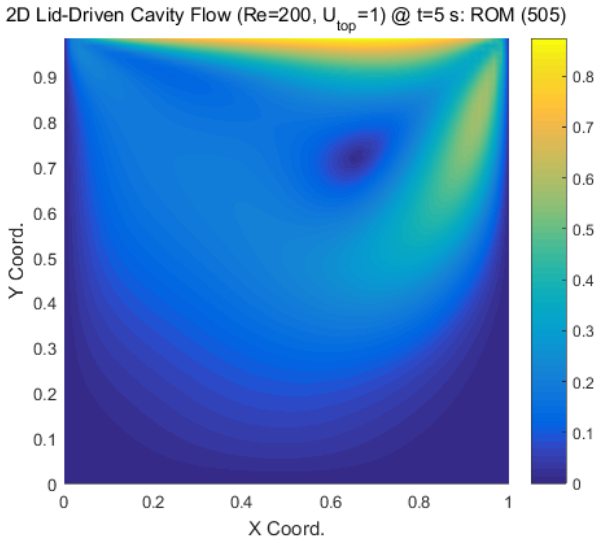

Figure 4 Velocity profile by ROM: $Re = 200$, $U_{top} = 1$ (nominal) at $t = 5\ sec$.

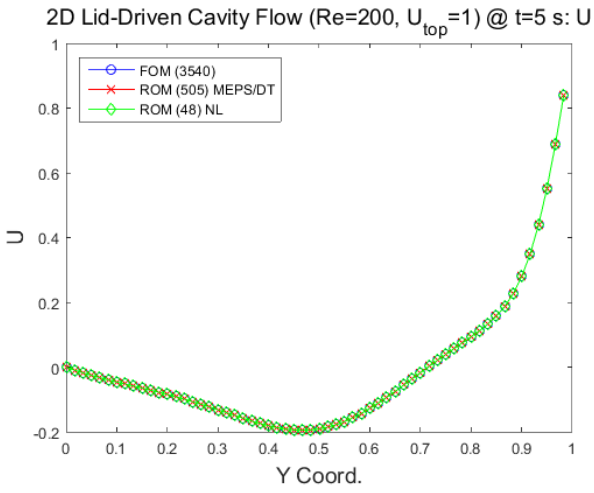

Figure 5 U velocity component: $Re = 200$, $U_{top} = 1$ (nominal) at $t = 5\ sec$

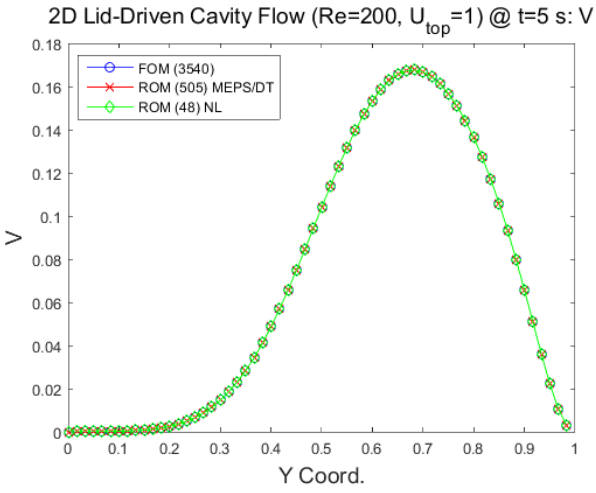

Figure 6 V velocity component: $Re = 200$, $U_{top} = 1$ (nominal) at $t = 5\ sec$

Figures 7 and 8 are velocity profiles for $Re = 400, U_{top} = 2$ at $t = 5\ sec$ based on the (3540×3540) FOM and the (505×505) ROM. Despite the doubling of the boundary speed, the two profiles match extremely well. Figures 9 and 10 are the two velocity components at the center of the cavity. Not surprisingly, the (48×48) ROM based on the nominal modes cannot approximate the FOM at this Reynolds number. That is, these modes are good and valid only for the very flow condition at which they were obtained.

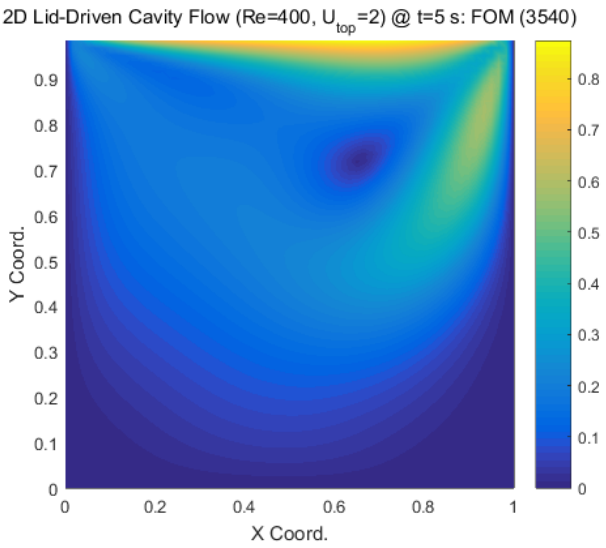

Figure 7 Velocity profile by FOM: $Re = 400$, $U_{top} = 2$ at $t = 5\ sec$.

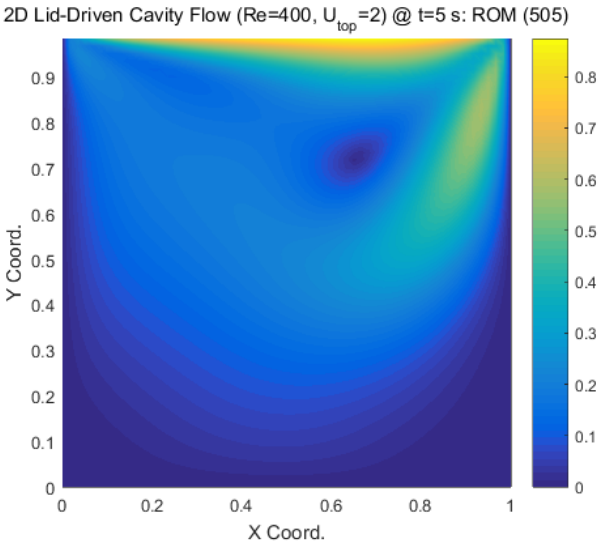

Figure 8 Velocity profile by ROM: $Re = 400$, $U_{top} = 2$ at $t = 5\ sec$.

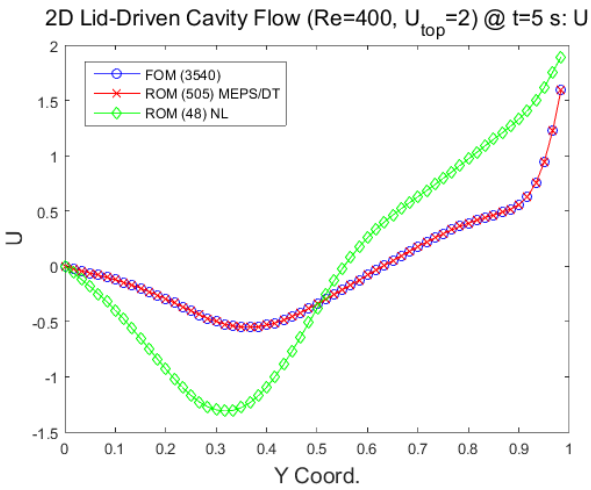

Figure 9 U velocity component: $Re = 400$, $U_{top} = 2$ at $t = 5\ sec$.

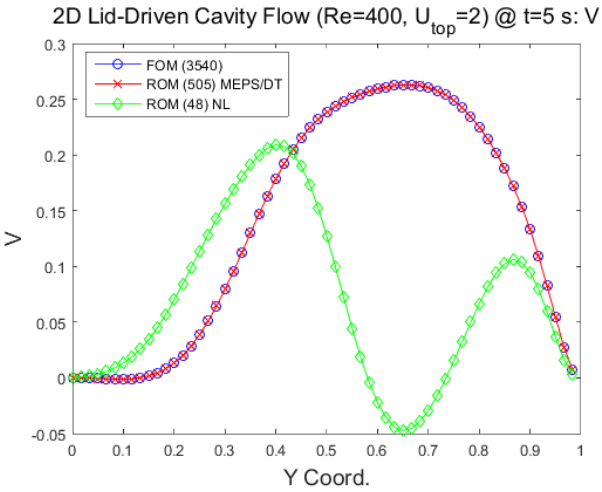

Figure 10 V velocity component: $Re = 400$, $U_{top} = 2$ at $t = 5\ sec$.

Figures 11 and 12 are velocity profiles for $Re = 600, U_{top} = 3$ at $t = 5\ sec$, Figures 13 and 14 are the two velocity components at the middle. Again, throughout the figures the (505×505) ROM is seen to be parametrically rich matching with the FOM very well, whereas the (48×48) ROM deviates substantially from the correct results. Due to a numerical stability requirement inherent in the CFD code it was not possible to go beyond Reynolds numbers greater than 600 with $\Delta t = .005\ sec$. This issue could be easily fixed by using a smaller time step. The last batch of figures, Figures 15-18 are for $Re = 100, U_{top} = .5$. Again, an excellent agreement is found between the FOM and the (505×505) ROM, but the (48×48) ROM fails to predict the flow field even if the boundary speed is lowered from the nominal value, all of which are an indication that the convective terms play a critical role and the flow field is very sensitive to the nonlinearity.

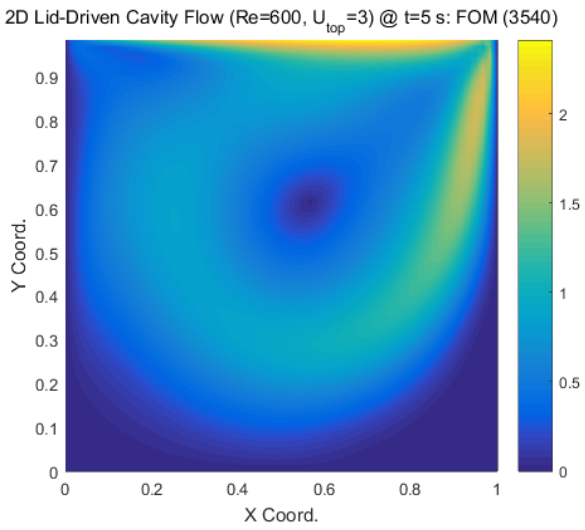

Figure 11 Velocity profile by FOM: $Re = 600$, $U_{top} = 3$ at $t = 5\ sec$.

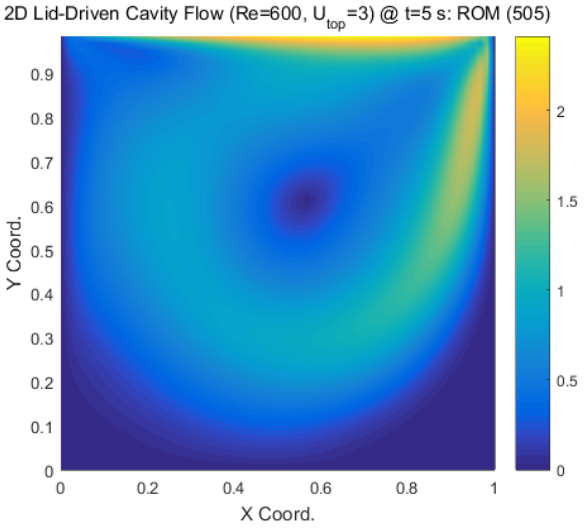

Figure 12 Velocity profile by ROM: $Re = 600$, $U_{top} = 3$ at $t = 5\ sec$.

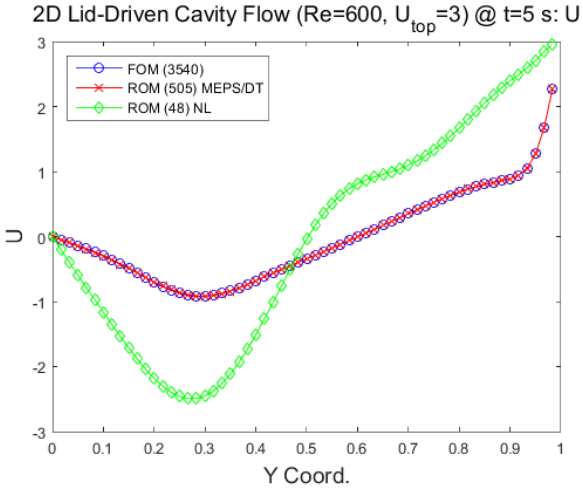

Figure 13 U velocity component: $Re = 600$, $U_{top} = 3$ at $t = 5\ sec$.

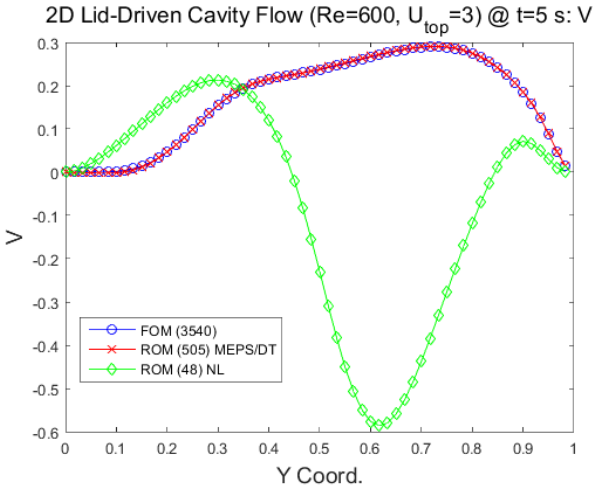

Figure 14 V velocity component: $Re = 600$, $U_{top} = 3$ at $t = 5\ sec$.

8. CONCLUDING REMARKS

In this work, we have sought parametrically rich basis vectors that can be used for analysis of nonlinear systems effectively allowing continuous variation of parameters and operating conditions. Towards this end, the nonlinear system equation was split into a nominal and a perturbed parts. The latter is transformed into a linear equation using two transformation techniques, namely the Modally Equivalent Perturbed System (MEPS) and the Degenerate Transformation (DT). When processed by Proper Orthogonal Decomposition (POD), solutions of the nominal and the perturbed systems together form a set of global modes for the nonlinear system. It was found that because they obey linear superposition, the basis vectors of the perturbed equation can span a rich nonlinear solution space covering multiple boundary conditions and inputs. That is, one does not need to repeat the calculations of POD modes for

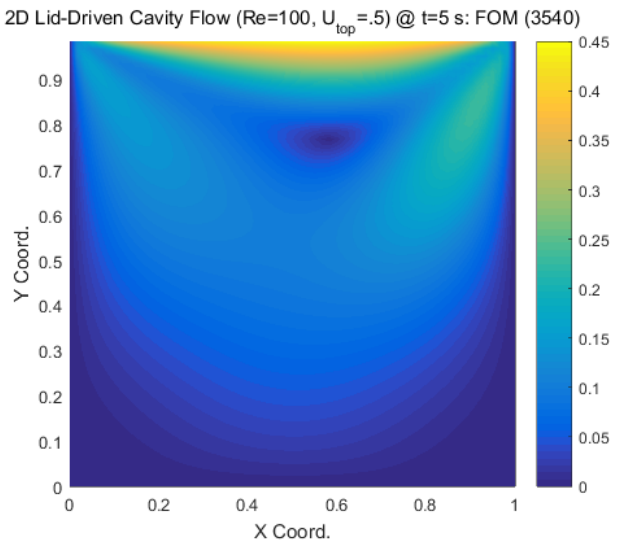

Figure 15 Velocity profile by FOM: $Re = 100$, $U_{top} = .5$ at $t = 5\ sec.$

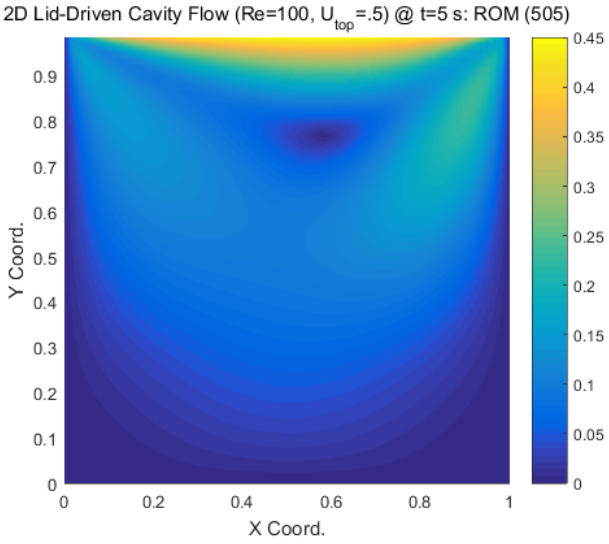

Figure 16 Velocity profile by ROM: $Re = 100$, $U_{top} = .5$ at $t = 5\ sec.$

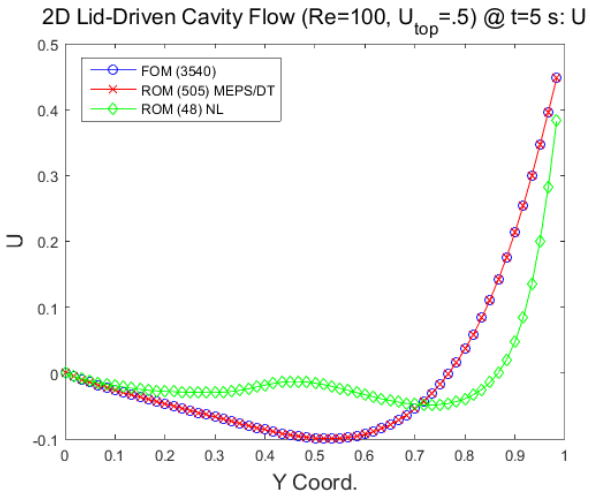

Figure 17 U velocity component: $Re = 100$, $U_{top} = .5$ at $t = 5\ sec.$

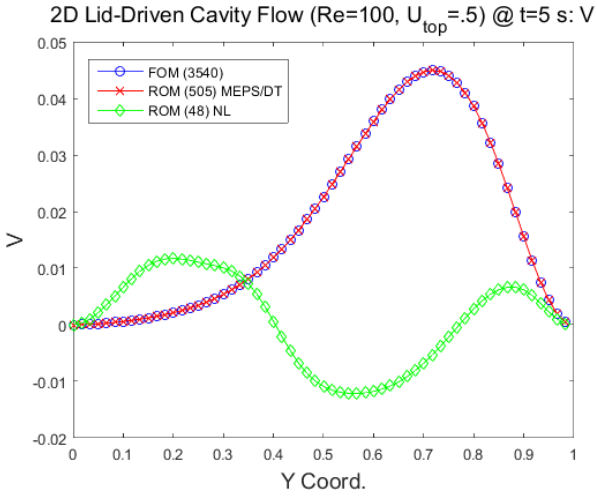

Figure 18 V velocity component: $Re = 100$, $U_{top} = .5$ at $t = 5\ sec.$

different conditions, as opposed to the aforementioned Greedy Sampling technique that is now often used in the literature. Naturally, this strategy invokes an efficient reduced-order modeling that can potentially save a significant computing time. The major difference between the previous research by the first author and the current work is that whereas the former assumes that the nonlinear system has an inherent linear part and formulates the perturbed equation in frequency domain, the latter treats systems that do not have explicit linear parts and hence formulates the perturbed system in time domain. The current scheme, therefore, has an advantage in that it can deal with nonlinear systems that do not have natural linear parts, e.g., the Euler equations of fluid mechanics.

The new scheme has been demonstrated using a computational model of a two-dimensional Lid-Driven Cavity Flow in which the basis modes were obtained from snapshots of time responses of the modified unsteady flow field. It is shown that the nonlinear reduced-order

model constructed from the calculated modes produce very accurate results for a wide range of Reynolds numbers and boundary speeds. In fact, because of the linearity of the basis functions, the MEPS/DT does not pose any limit in principle on how much of the parameter space the modes can span. In this regard and others, it is worthwhile to revisit the four questions raised at the end of Section 2, particularly the first and the third questions:

- How should $\boldsymbol{T}(\omega)$ be formulated in a meaningful way such that (3) effectively covers the range of variations in the parameters and operating conditions?
- Are there alternatives to $\boldsymbol{v}_{\mathrm{i}}(t)$'s because executing the convolutions as given in (3) could be computationally expensive?

In fact, throughout the course of the current and previous cited research works, the frequency valued transfer function of the perturbed system has been used for $\boldsymbol{T}(\omega)$. In the case of linear systems, this is equal to the transfer function from the nominal solution to the perturbed solution. In the case of nonlinear system, it is a transfer function from a linear or a nonlinear nominal solution to the perturbed solution. As for the other question, the dynamic eigenmodes $\boldsymbol{v}_{\mathrm{i}}(t)$'s have been replaced with static modes, $\boldsymbol{\phi}_{\mathrm{i}}$'s via the POD procedure.

There remain several questions and issues that need to be addressed and answered in future research. First, the number of modes, 505 seems very large compared to the number of nominal modes, 48. One may argue that this is because the scheme seeks all the modes that are necessary to capture for the entire range of nonlinear operating conditions. Still, it will be useful to control the range of the conditions, hence the number of modes. One option would be, after getting $\boldsymbol{\phi}_{\mathrm{i}}$'s, to perform POD on the modes specifically for a given fixed condition. This will result in a reduced set of modes of a much smaller size good for the fixed condition. Second, using randomly distributed signals $r_{0i}(t)$'s in $\boldsymbol{\Delta A}(\boldsymbol{\Phi}_0\boldsymbol{r}_0)$ is not in general recommended, especially if it involves running an advanced CFD code. This is because CFD solvers are highly sensitive to noisy inputs and do not converge well under such an excitation. One might have to use an alternative signal such as a smoothed random or a Gaussian input. Lastly and most importantly, it will be necessary to demonstrate the method for nonlinear systems that exhibit severe nonlinearities, such as turbulent flows, compressible flows, transonic flows with shocks, etc.

9. REFERENCES

[1] Frangos, M., Marzouk, Y., Willcox, K., Waanders, B.V.B., Surrogate and Reduced-Order Modeling: A Comparison of Approaches for Large-Scale Statistical Inverse Problems. Large-Scale Inverse Problems and Quantification of Uncertainty. Chapter 7, 2011, 123-149, John Wiley & Sons Ltd.

[2] Paul-Dubois-Taine, A., Amsallem, D., An Adaptive and Efficient Greedy Procedure for the Optimal Training of Parametric Reduced-Order Models. International Journal for Numerical Methods Engineering 2014, 00, 1–32.

[3] Kim, T., Finding Parametrically Rich Nonlinear Solution Space Using Degenerate Transformation, submitted to International Journal of Numerical Methods in Engineering, 2017.

[4] Kim, T., Surrogate Model Reduction for Linear Dynamic Systems Based on a Frequency Domain Modal Analysis. Computational Mechanics 2015, 56 (4), 709-723.

[5] Kim T., Parametric model reduction for aeroelastic systems: Invariant aeroelastic modes, Journal of Fluids and Structures 2016, 65: 196-216.

[6] Kim, T., Frequency Domain Karhunen-Loeve Method and Its Application to Linear Dynamic Systems, AIAA Journal, Vol. 36, No. 11, 1998, pp. 2117-2123.

[7] Hall, K., Thomas, J.P., Dowell, E.H., Proper Orthogonal Decomposition Technique for Transonic Unsteady Aerodynamic Flows. AIAA Journal 2000, 38 (10), 1853–1862.

[8] Tomas-Rodriguez, M., Banks, S.P., Linear, Time-varying Approximations to Nonlinear Dynamical Systems: with Applications in Control and Optimization, Springer, 2010.

[9] Chen, C.T., Linear System Theory and Design. 4th Ed., Oxford University Press. 2012, Oxford.

[10] Chaturantabut , S., Sorensen, D.C., Application of POD and DEIM on Dimension Reduction of Nonlinear Miscible Viscous Fingering in Porous Media, Technical Report: CAAM, Rice University, R09-25, 2009.

[11] Peherstorfer, B., Butnaru, D., Willcox, K., Bungart, H.J., Localized Discrete Empirical Interpolation Method, MIT Aerospace Computational Design Laboratory Technical Report TR-13-1, June 2013.

[12] Balajewicz1,M.J., Dowell, E.H., Noack, B.R., Low-dimensional modelling of high-Reynolds-number shear flows incorporating constraints from the Navier–Stokes equation, J. Fluid Mech. (2013), vol. 729, pp. 285–308.

[13] Balajewicz1,M.J., Tezaur, I., Dowell, E.H., Minimal subspace rotation on the Stiefel manifold for stabilization and enhancement of projection-based reduced order models for the compressible Navier–Stokes equations, Journal of Computational Physics 321 (2016) 224–241.

10. COPYRIGHT STATEMENT